International Journal of Minerals, Metallurgy and Materials
Volume 23, Number 1, January 2016, Page 57
DOI: 10.1007/s12613-016-1211-6

Effects of normal stress, surface roughness, and initial grain size on the microstructure of copper subjected to platen friction sliding deformation

Shan-quan Deng, Andrew-William Godfrey, Wei Liu, Cheng-lu Zhang, and Ben Xu

Key Laboratory of Advanced Materials (MOE), School of Materials Science and Engineering, Tsinghua University, Beijing 100084, China
(Received: 22 May 2015; revised: 19 August 2015; accepted: 1 September 2015)

Abstract: The effects of applied normal stress, surface roughness, and initial grain size on the microstructure of pure Cu developed during platen friction sliding deformation (PFSD) processing were investigated. In each case, the deformation microstructure was characterized and the hardness of the treated surface layer was measured to evaluate its strength. The results indicated that the thickness of the deformed layer and the hardness at any depth increased with increasing normal stress. A smaller steel platen surface roughness resulted in less microstructural refinement, whereas the microstructural refinement was enhanced by decreasing the surface roughness of the Cu sample. In the case of a very large initial grain size (d > 10 mm), a sharper transition from fine-grain microstructure to undeformed material was obtained in the treated surface layer after PFSD processing.

Keywords: copper; surface treatment; processing parameters; grain refinement; gradient microstructure; hardness

1. Introduction

The generation of gradient structures has recently been the subject of extensive research [1–4], which has confirmed that the surface modification of metals by generating a gradient nanostructure can improve surface properties such as diffusion behavior, as well as wear and corrosion, and fatigue resistance [5–10]. Such improvements are very important for increasing the service life of engineering materials because many failures originate at or near the material's surface. One approach to achieving the formation of a surface gradient nanostructure is sliding deformation, and several studies describing the use and results of this technique have been published [11–15]. The fine microstructure developed in a surface layer treated by sliding deformation has been reported to reduce the wear rate and the friction coefficient at the material surface [16–17]. Thus, control of the fine microstructure generated by sliding is important for optimizing the surface properties of materials as well as for guiding further applications of this technique.

The processing parameters of sliding deformation will undoubtedly affect the generated microstructure. Other authors have reported that an increase in sliding velocity will generate a thinner near-surface tribolayer consisting of a fine microstructure (even down to the nanoscale) during unlubricated sliding of Cu [18]. Moreover, dynamic recrystallization has been reported to interrupt the formation of a continuous nanocrystalline tribolayer at high sliding velocities [19]. Zhang *et al.* [14] studied the effect of applied load during ball-on-disc sliding of Cu and Ta and reported an increase in the thickness of the deformed layer with increasing normal load. Other researchers have demonstrated that the minimum scale of the microstructure in Cu subjected to sliding using a flat platen can be reduced by carrying out the sliding at liquid-nitrogen temperature and by subjecting the sample to a pre-alloying treatment [20].

In the present study, we investigated the influence of several processing and material parameters (specifically, applied normal load, surface roughness, and sample grain size) on the microstructure developed during platen friction sliding deformation (PFSD) of pure Cu at room temperature. In each case, the microstructure was characterized and the influence on the mechanical properties was analyzed via hardness measurements.

Corresponding author: Andrew-William Godfrey E-mail: awgodfrey@mail.tsinghua.edu.cn

2. Experimental

The main material used in this study was oxygen-free high-conductivity (OFHC) Cu with a purity of 99.9%, in a fully recrystallized condition with an average grain size of 73 μm (not counting annealing twins as individual grains) and a nearly random texture. The PFSD processing, as shown in Fig. 1, was performed using a specially designed rig. In general, the Cu sample was first pressed against a stainless steel platen with a preset normal stress, forming a plane–plane contact configuration; the sample and platen dimensions were 11.5 mm × 11.5 mm × 9 mm and 32 mm × 32 mm × 100 mm, respectively. Using a loading frame, we subsequently slid the steel platen against the Cu sample with a sliding speed of 6.7 $mm \cdot s^{-1}$ at room temperature. In each case, a sliding distance of approximately 60 mm was used, resulting in the formation of a friction-induced shear deformation in the surface layer of the Cu sample. After PFSD, all samples were stored at −18°C in a freezer to prevent recovery and recrystallization during storage.

For the reference sample R used in this study, the normal applied stress was 44 MPa and the surface roughness values of the contact surfaces of the Cu sample and the steel platen before PFSD were R_a = 5.1 μm and R_a = 3.2 μm, respectively. To study the effects of normal stress and surface roughness on the microstructure obtained after PFSD processing, different normal stress and surface roughness (for both the Cu sample and the steel platen) were also used. In addition, another Cu sample (also 99.9% purity) with a very large grain size, determined to be greater than 13 mm, was used to study the effect of initial grain size. The detailed deformation parameters for each sample are listed in Table 1.

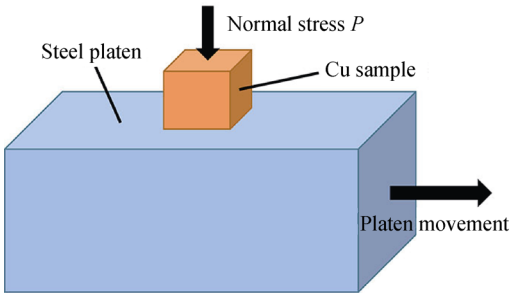

Fig. 1. Schematic showing the relative movement of the steel platen and Cu sample during PFSD processing.

Table 1. Summary of platen friction sliding deformation conditions for investigated samples

Sample	Normal stress, P / MPa	Sliding distance / mm	Notes
R	44	62	Reference sample (R_a(steel) = 3.2 μm, R_a(Cu) = 5.1 μm)
1	22	60	Small normal force
2	88	59	Large normal force
3	44	60	Smoother steel block (R_a = 0.9 μm)
4	44	58	Smoother Cu sample (R_a = 0.1 μm)
5	44	59	Larger initial grain size (13. 8 mm)

For each sample, the microstructure of the treated surface layer after PFSD was characterized in cross-section (i.e., the plane perpendicular to the friction surface and containing the sliding direction) using a Tescan Mira 3 LMH thermal field emission scanning electron microscope equipped with an Oxford Instruments HKL Nordlys Max electron backscatter diffraction (EBSD) system. To avoid external-stress-induced damage (i.e., chamfer) on the surface-deformed layer during grinding on the cross-section, a small block of Cu was adhered to the treated surface of the Cu sample using glue. The cross-section of the Cu sample together with the Cu block was then vibration-polished after being ground to remove the stress influence during grinding. After the sample was polished, the Cu block was removed by ultrasonic cleaning in acetone and alcohol, and the Cu sample was observed by scanning electron microscopy (SEM). The hardness of the treated surface layer was investigated by Vickers micro-hardness indentation using a load of 10 g and a duration of 10 s.

3. Results and discussion

3.1. General microstructure in Cu after PFSD

A typical gradient nanostructure was generated in the surface layer of Cu subjected to PFSD at room temperature, as we demonstrated in a previous study [21]. Fig. 2 shows the general microstructure profile along the depth from the Cu friction surface subjected to PFSD. In brief, four regions are observed, each with a different typical morphology of the deformed microstructure. From the friction surface to the interior matrix, these four microstructures are (1) a nanoscale lamella microstructure in which the lamellae are nearly parallel to the sliding direction and exhibit an average spacing of approximately 50–100 nm; (2) a fine-grain microstructure in which most of the fine grains are elongated along the sliding direction and exhibit an average spacing (measured perpendicular to the friction surface) of approximately 300 nm; (3) a regular lamellar deformation microstructure in which long bands are also elongated predominantly along

the sliding direction and in which the band spacing increases with increasing depth from the friction surface; and (4) a deformed-grain microstructure in which the initial grains are clearly evident and show evidence of the introduction of plastic deformation, where the amount of plastic deformation decreases with increasing depth from the friction surface.

These four types of microstructures are illustrated in the cross-section of the reference sample R shown in Fig. 3. The top 200 μm layer of this sample exhibits a very clear plastic-deformation-induced gradient structure morphology, where clear shearing is still observed at a depth of at least 100 μm (Fig. 3(a)). The top 40 μm layer has obviously been severely refined (Fig. 3(b)). Moreover, the top 30 μm layer fully consists of the fine-grain microstructure (Figs. 3(b) and 3(d)), except for a very thin layer of nanoscale lamellae at the top surface. The microstructural morphology of these fine grains is shown in Figs. 3(c) and 3(e), which show the microstructures observed at depths of 10 μm and 20 μm, respectively. Most of these fine grains are elongated along the sliding direction, although some smaller grains with a more equiaxed shape are also observed. Many of the fine grains do not contain interior misorientations, and most are enclosed by high-angle boundaries (with misorientation angles ≥ 15°). Moreover, little difference is observed between the morphologies of the fine grains developed over this region (see Figs. 3(c) and 3(e)).

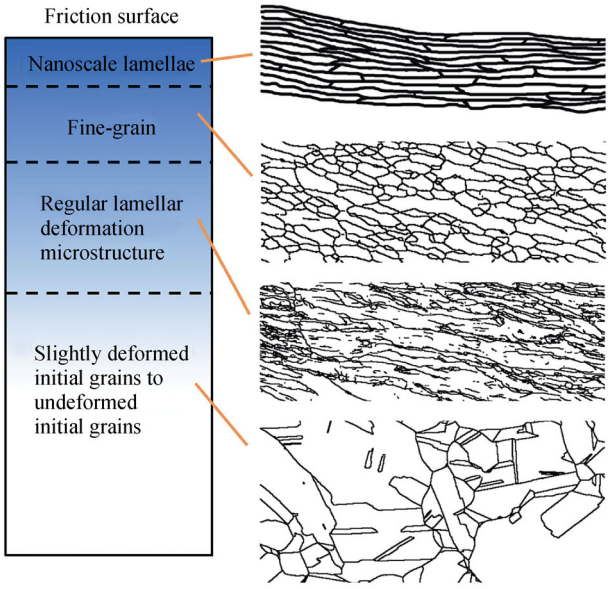

Fig. 2. Schematic of the general microstructure profile as a function of depth from the treated surface for Cu subjected to PFSD.

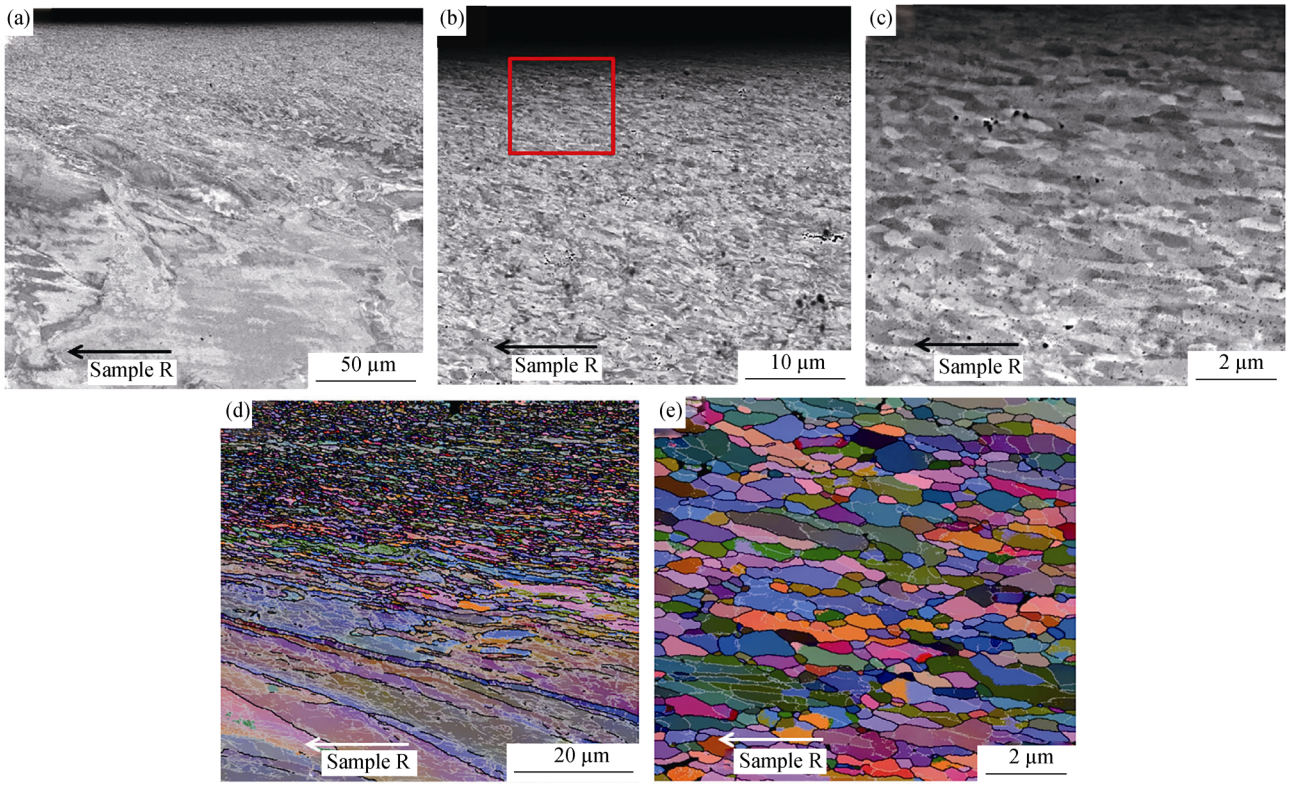

Fig. 3. Microstructure of sample R (reference sample) viewed in cross-section by SEM and EBSD: (a) top 200 μm layer; (b) top 40 μm layer; (c) magnified image corresponding to the red box in (b); (d) top 70 μm layer; (e) 15–25 μm layer. Grey and black lines in the EBSD maps indicate boundaries with misorientation ≥ 1.5° and ≥ 15°, respectively. Arrows indicate the sliding direction of the steel platen.

3.2. Effect of normal stress

3.2.1. Microstructural morphology

Figs. 4 and 5 present examples of microstructural morphologies viewed in the cross-sections of samples 1 and 2 by SEM and EBSD, respectively. Compared with the stress used to deform the reference sample, during PFSD, sample 1 was deformed with a smaller normal stress (22 MPa),

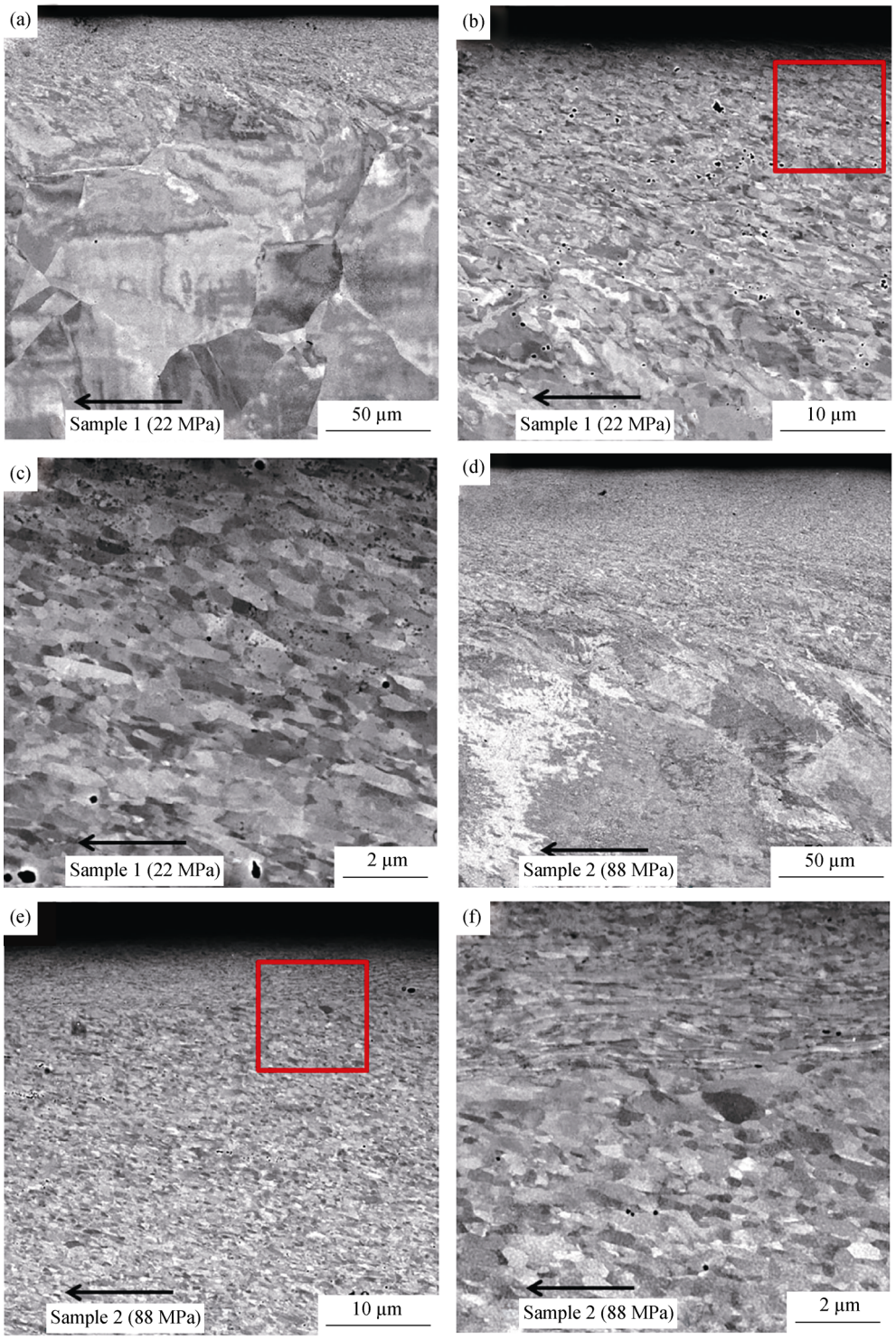

Fig. 4. Microstructures of samples 1 and 2 (showing the effect of normal stress) viewed in cross-section by SEM: (a, d) top 200 μm layer; (b, e) top 40 μm layer; (c, f) magnified images corresponding to red boxes in (b) and (e), respectively. Arrows indicate the sliding direction of the steel platen.

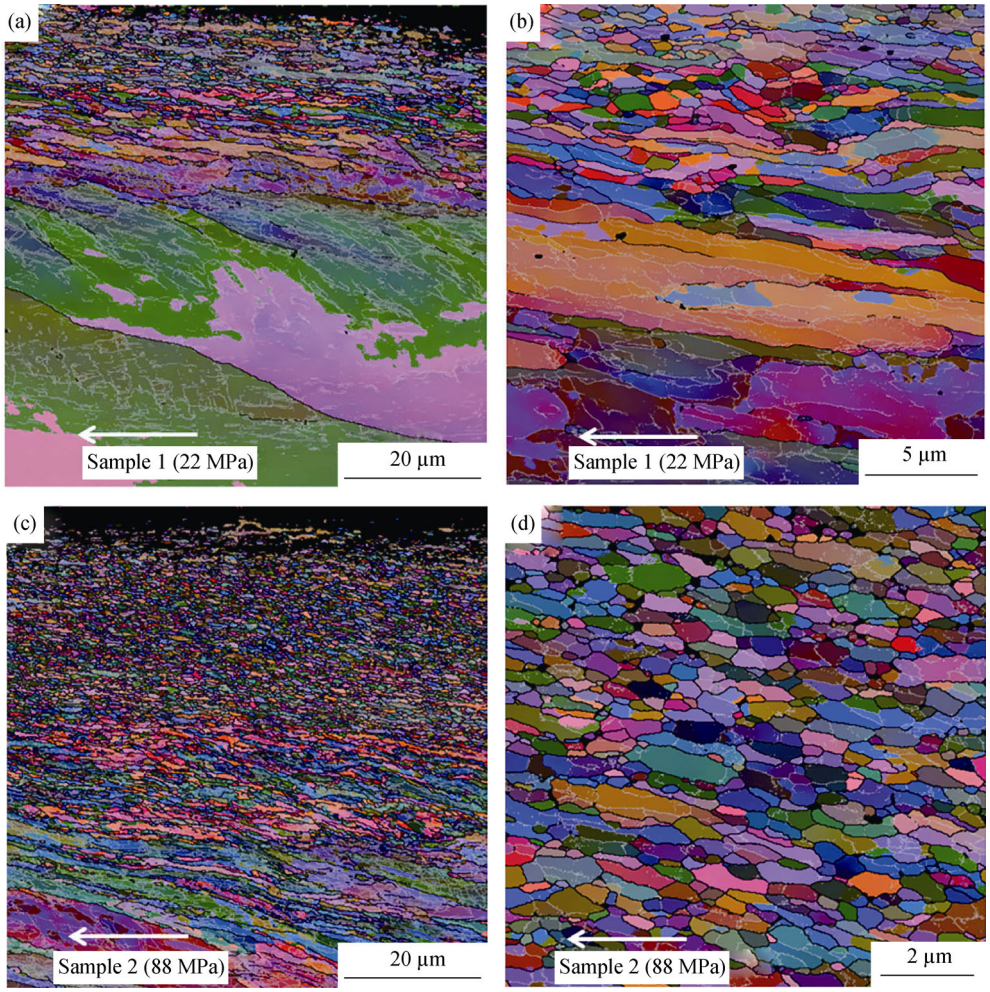

Fig. 5. Microstructures of samples 1 and 2 viewed in cross-section by EBSD: (a, c) top 70 μm layer; (b) 10–30 μm layer in sample 1; (d) 15–25 μm layer in sample 2. Grey and black lines in the EBSD maps indicate boundaries with misorientation ≥ 1.5° and ≥ 15°, respectively. Arrows indicate the sliding direction of the steel platen.

whereas sample 2 was deformed with a larger normal stress (88 MPa). As evident in Fig. 4(a), less plastic deformation was introduced into the surface layer of sample 1, and the maximum depth where clear shearing is evident was only approximately 75 μm. In addition, only a thin, severely refined layer containing the fine-grain microstructure was generated (Fig. 5(a)). In contrast, larger plastic deformation was introduced into the surface layer of sample 2, and shearing was clearly visible even at a depth of 135 μm (Fig. 4(d)). A thicker severely refined (fine-grained) layer was also observed (Fig. 5(c)). The thickness of the layer comprising fine grains in sample 1 was only approximately 15 μm (Fig. 4(b)), whereas the top 40 μm layer in sample 2 consisted almost entirely of fine grains (Fig. 4(e)).

This difference in the thickness of the fine-grained layer was also evident from the microstructure at a depth of 20 μm, as shown in Figs. 5(b) and 5(d). In Fig. 5(b) (sample 1 with lower normal stress), a regular lamellar deformation microstructure with quite coarse spacing was observed at 20 μm depth, whereas fine grains were still evident at the same depth in sample 2 (higher applied stress). Moreover, a larger fraction of the fine grains was smaller and more equiaxed in sample 2 compared with that in sample R. On the basis of these observations, we concluded that both the maximum depth of shearing and the thickness of the fine-grained layer increased with increasing normal stress.

Figs. 4(c) and 4(f) show the microstructures of samples 1 and 2 at 10 μm depth, respectively. The microstructure shown in Fig. 4(c) is almost composed of fine grains, similar to that of sample R (Fig. 3(c)). However, a large difference was observed in sample 2, where a nanoscale lamella microstructure was observed at a depth of approximately 10 μm (Fig. 4(f)). The generation of a nanoscale lamella microstructure confirms the hypothesis that more plastic deformation must have been introduced into sample 2 than sample R, i.e., microstructural refinement was enhanced using a larger normal stress.

3.2.2. Spacing and hardness

Fig. 6 shows the variation of the average spacing of high-angle boundaries at 20 μm depth and of the hardness at certain depths as functions of normal stress. Here, the spacing of high-angle boundaries was measured perpendicular to the sliding direction on the basis of EBSD characterization. In general, the spacing at this depth decreased with increasing normal stress (Fig. 6(a)). More specifically, the spacing significantly decreased as the normal stress increased from 22 MPa (sample 1) to 44 MPa (sample R), whereas it decreased only slightly as the normal stress was further increased from 44 MPa (sample R) to 88 MPa (sample 2). The results of these measurements are consistent with the microstructures shown in Figs. 3(e), 5(b), and 5(d). Moreover, the hardness values measured at 40 μm depth, 20 μm depth, and the friction surface (Fig. 6(b)) increased with increasing normal stress. However, at 40 μm and 20 μm depths, the increase in hardness was small. For example, the hardness at 20 μm depth only increased from 1.15 GPa in sample 1 to 1.26 GPa in sample 2.

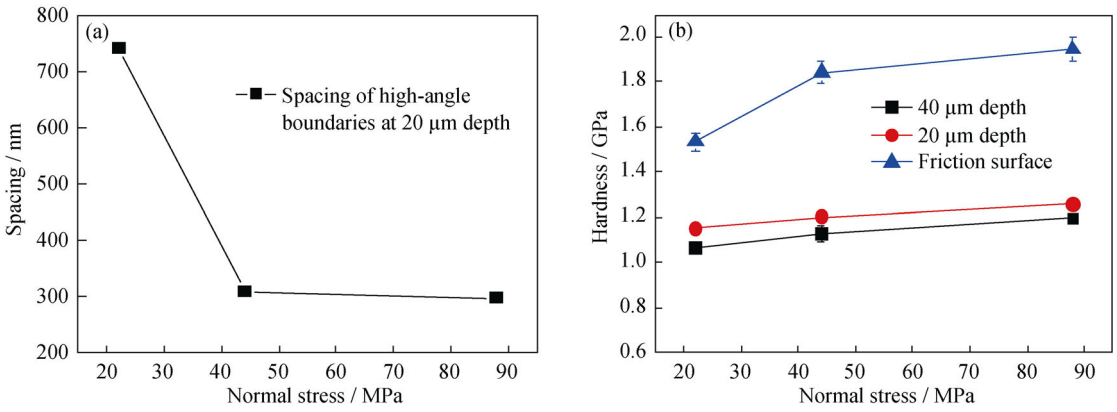

Fig. 6. Effect of normal stress on the spacing of high-angle boundaries at 20 μm depth (a) and the hardness at fixed depths (b).

Apparently, the friction force will definitely increase with increasing normal stress as long as contact conditions remain unchanged. Moreover, the friction coefficient is known to increase with increasing normal stress [22], which can further increase the friction force acting on the treated surface of the Cu sample. Therefore, the treated surface of the Cu sample will suffer more severe plastic deformation, and the evolution of the microstructure will be accelerated when a larger normal stress is applied. Accordingly, more fine grains are formed and even more nanoscale lamellae appear in the treated surface layer. Furthermore, the formation of fine grains and nanoscale lamellae has been reported to lead to a transfer of shear strain to deeper volumes [21]. Thus, the thicknesses of the fine-grained and deformed layers increase with increasing normal stress, as does the hardness.

3.3. Effect of surface roughness

3.3.1. Microstructural morphology

Figs. 7 and 8 show examples of the microstructural morphology viewed in cross-sections by SEM and EBSD, respectively, for samples deformed under different surface roughness conditions. Sample 3 was deformed with a relatively smoother steel platen surface with R_a = 0.9 μm, which is only approximately one-third the R_a of the steel platen surface used for sample R. In the case of sample 4, the surface of the Cu sample was electropolished before PFSD processing, resulting in a smaller surface roughness of R_a = 0.1 μm.

The top 200 μm layer of sample 3 (Fig. 7(a)) exhibited a substantially different microstructural morphology compared with that observed over the same depth in sample R, with only a very small amount of severe plastic deformation introduced in the surface layer. The maximum depth where shearing was evident was only approximately 25 μm (all annealing twin boundaries beneath this depth were still very straight), and all original grains were still clearly recognizable, with no obvious shape change below a depth of 25 μm. Moreover, neither a nanoscale lamella layer nor a fine-grained layer was formed during PFSD in this sample (Fig. 7(b)). An examination of the EBSD data revealed that grain subdivision only occurred in the top 10 μm layer, as indicated by newly formed high-angle boundaries only being observed above this depth (Fig. 8(b)). In this layer, a regular lamellar deformation microstructure was formed, although this microstructure was still in the early stage of development. In addition, little evidence of plastic deformation was observed at depths greater than 10 μm, as inferred from the very small number of observed low-angle boundaries with misorientation angles between 1.5° and 15° (Fig.

8(a)). Thus, the decrease of the steel platen surface roughness significantly retarded the evolution of the nanoscale microstructure during PFSD.

In sample 4, the microstructural morphology in the top 200 μm layer exhibits features similar to that of sample R (Fig. 7(c)). In this sample, direct evidence of shearing is observed but at a depth of 120 μm, i.e., at a greater depth than the shearing in sample R. The top 40 μm layer of sample 4 is severely refined (Fig. 7(d)), with a fine-grain microstructure (Fig. 8(c)) observed at a depth of 30 μm. However, the fine grains at 20 μm depth in sample 4 (Fig. 8(d)) are approximately the same in terms of size and shape as those at a similar depth in sample R (Fig. 3(e)). A significant difference in sample 4 is the development of a highly refined

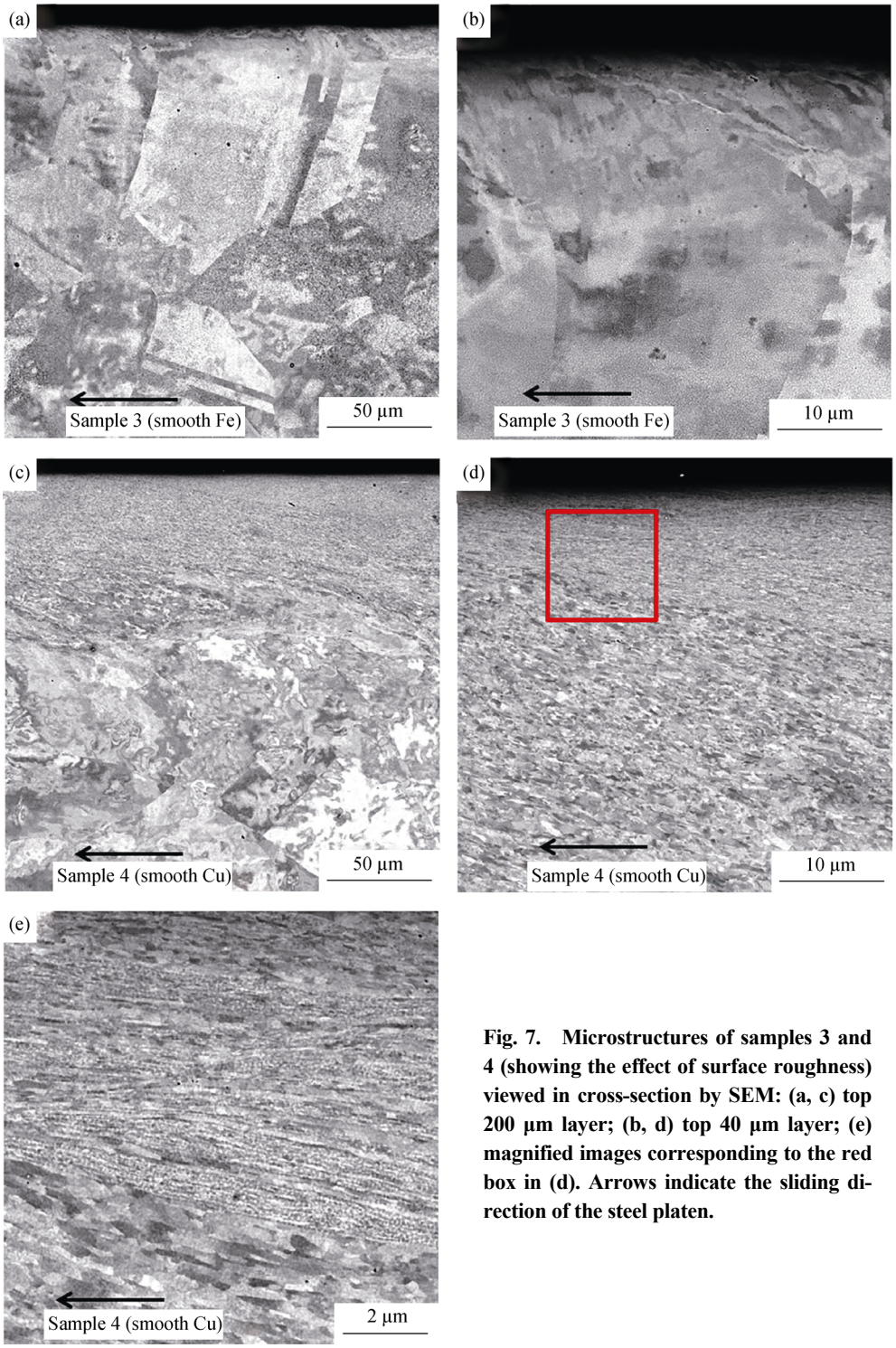

Fig. 7. Microstructures of samples 3 and 4 (showing the effect of surface roughness) viewed in cross-section by SEM: (a, c) top 200 μm layer; (b, d) top 40 μm layer; (e) magnified images corresponding to the red box in (d). Arrows indicate the sliding direction of the steel platen.

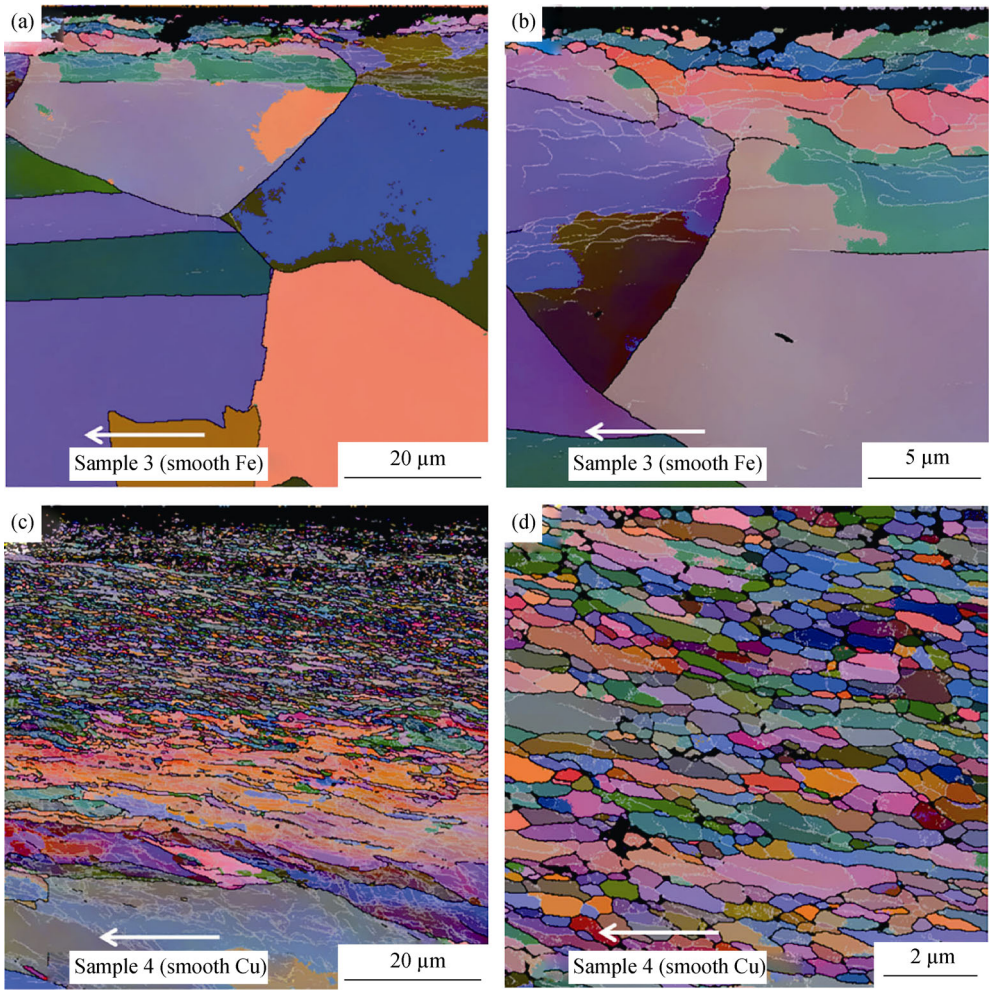

Fig. 8. Microstructures of samples 3 and 4 viewed in cross-section by EBSD: (a, c) top 70 μm layer; (b) top 20 μm layer in sample 3; (d) 15–25 μm layer in sample 4. Grey and black lines in the EBSD maps indicate boundaries with misorientation ≥ 1.5° and ≥ 15°, respectively. Arrows indicate the sliding direction of the steel platen.

microstructure in the top 15 μm layer (Fig. 7(d)). A relatively higher magnification observation reveals that this layer comprises the nanoscale lamella microstructure (Fig. 7(e)). In addition, some regions of this microstructure are sandwiched within the fine-grain microstructure. Notably, the maximum depth at which the lamella microstructures are observed in sample 4 is greater than that in sample 2. Therefore, a decrease of the Cu sample surface roughness can substantially enhance the evolution of the nanoscale microstructure.

3.3.2. Spacing and hardness

Figs. 9(a) and 9(b) show the hardness variation at a fixed depth as a function of the steel platen surface roughness and the Cu sample surface roughness, respectively. The hardness values at 40 μm depth, 20 μm depth, and the friction surface decrease drastically with decreasing steel platen surface roughness, whereas the hardness values increase with decreasing Cu sample surface roughness. These trends are consistent with the changes observed in the microstructures among samples R, 3, and 4. As shown in Fig. 8(b), for sample 3, no new high-angle boundaries is formed below a depth of 20 μm; thus, the data for the spacing of high-angle boundaries at this depth are not available. Fig. 9(c) shows the variation of the spacing of high-angle boundaries at 20 μm depth as a function of the Cu sample surface roughness. The spacing decreases only slightly with decreasing Cu sample surface roughness, which is in good agreement with the similar microstructures shown in Figs. 3(e) and 8(d).

On the basis of the aforementioned results, we concluded that the steel platen surface roughness plays a more important role than the Cu sample surface roughness in the evolution of the microstructure. As the Cu sample is pressed against the steel platen with certain normal stress, the asperities of the platen will indent to a certain depth (estimated as several to ten micrometers in the case presented here) into the Cu sample surface layer. Therefore, when the surface

roughness of the platen decreases (i.e., when the asperities of the platen become less pronounced), the indentation depth will decrease. Consequently, the friction force that results in the plowing of the Cu sample surface decreases, and therefore, less plastic deformation is introduced. In contrast, the indentation depth will increase if the surface roughness of the Cu sample decreases. In this case, the friction force will be greater, and more plastic deformation will consequently be introduced. Because the sample (Cu) is much softer than the steel platen, the asperities of the platen remain largely unchanged compared with those at the Cu sample surface during loading. As a result, when compared with the Cu sample surface, the PFSD process is more sensitive to the variation in the asperities of the steel platen.

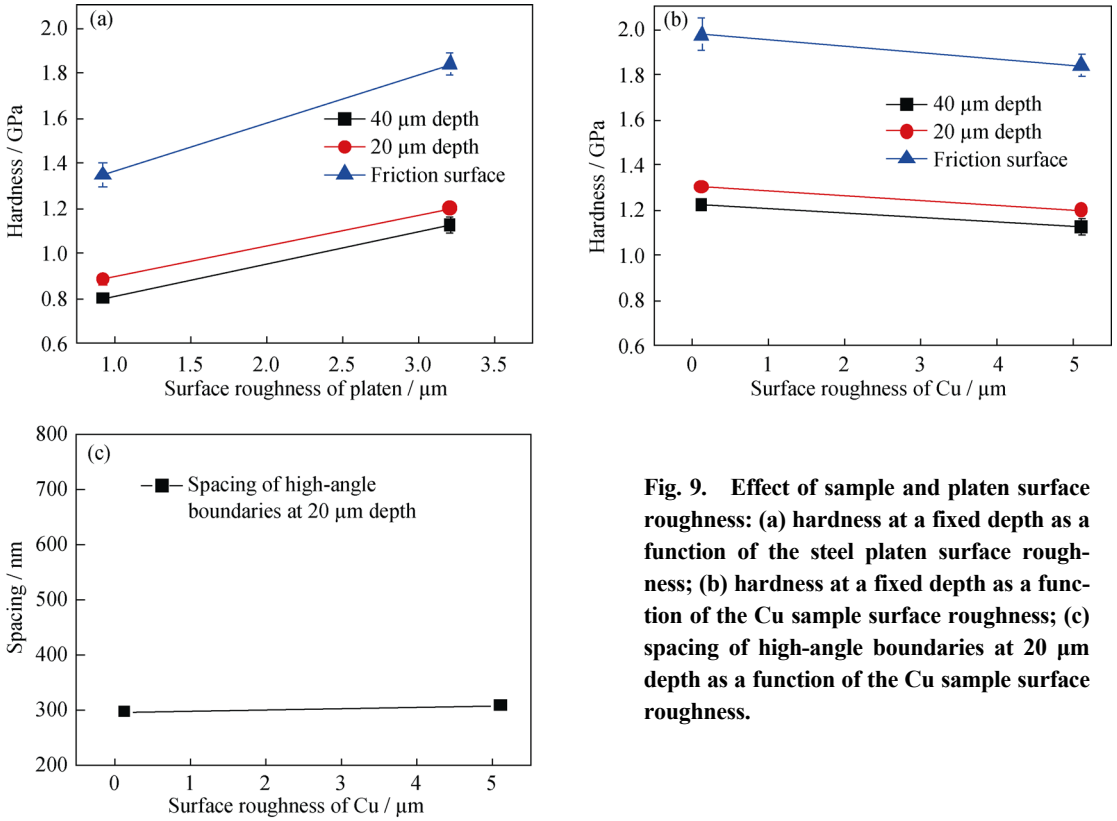

Fig. 9. Effect of sample and platen surface roughness: (a) hardness at a fixed depth as a function of the steel platen surface roughness; (b) hardness at a fixed depth as a function of the Cu sample surface roughness; (c) spacing of high-angle boundaries at 20 μm depth as a function of the Cu sample surface roughness.

In a previous study, it has been concluded that the friction coefficient on a smooth sample surface is larger than that on a rough sample surface [23]. Moreover, Leu [24] has reported that the friction coefficient will obviously increase when the relative roughness (i.e., the ratio between the roughness of the tool and that of the workpiece) increases during dry-contact friction. In the present case, the steel platen represents the tool, and the Cu sample represents the workpiece. Therefore, the decrease of the surface roughness of the steel platen will decrease the friction coefficient, whereas the decrease of the surface roughness of the Cu sample will increase the friction coefficient. As discussed in Section 3.2, a large friction coefficient will lead to significant plastic deformation in the treated surface. As a result, a decrease of the surface roughness of the steel platen can hinder the evolution of the nanoscale microstructure, whereas a decrease of the surface roughness of the Cu sample can enhance the evolution of the nanoscale microstructure during PFSD.

3.4. Effect of initial grain size

3.4.1. Microstructural morphology

The microstructural morphology observed in the cross-section of sample 5 is shown in Fig. 10. Sample 5 exhibits a much larger initial grain size, approximately 13.8 mm, compared to sample R. In this sample, the upper 40 μm layer is clearly refined, whereas below this depth the microstructure is less refined (Fig. 10(a)), as evidenced by the lack of high-angle boundaries and by the clear shape of the original grains. The top 10 μm layer consists of a fine-grain microstructure (Figs. 10(b) and 10(c)) very similar to that observed in sample R. Below this 10 μm depth, a regular lamellar deformation microstructure is already observed (Figs. 10(d)). In contrast to sample R, the regular lamellar deformation microstructure only extends over a depth of 30 μm. At greater depths, a fairly sharp transition to a deformed-grain region is

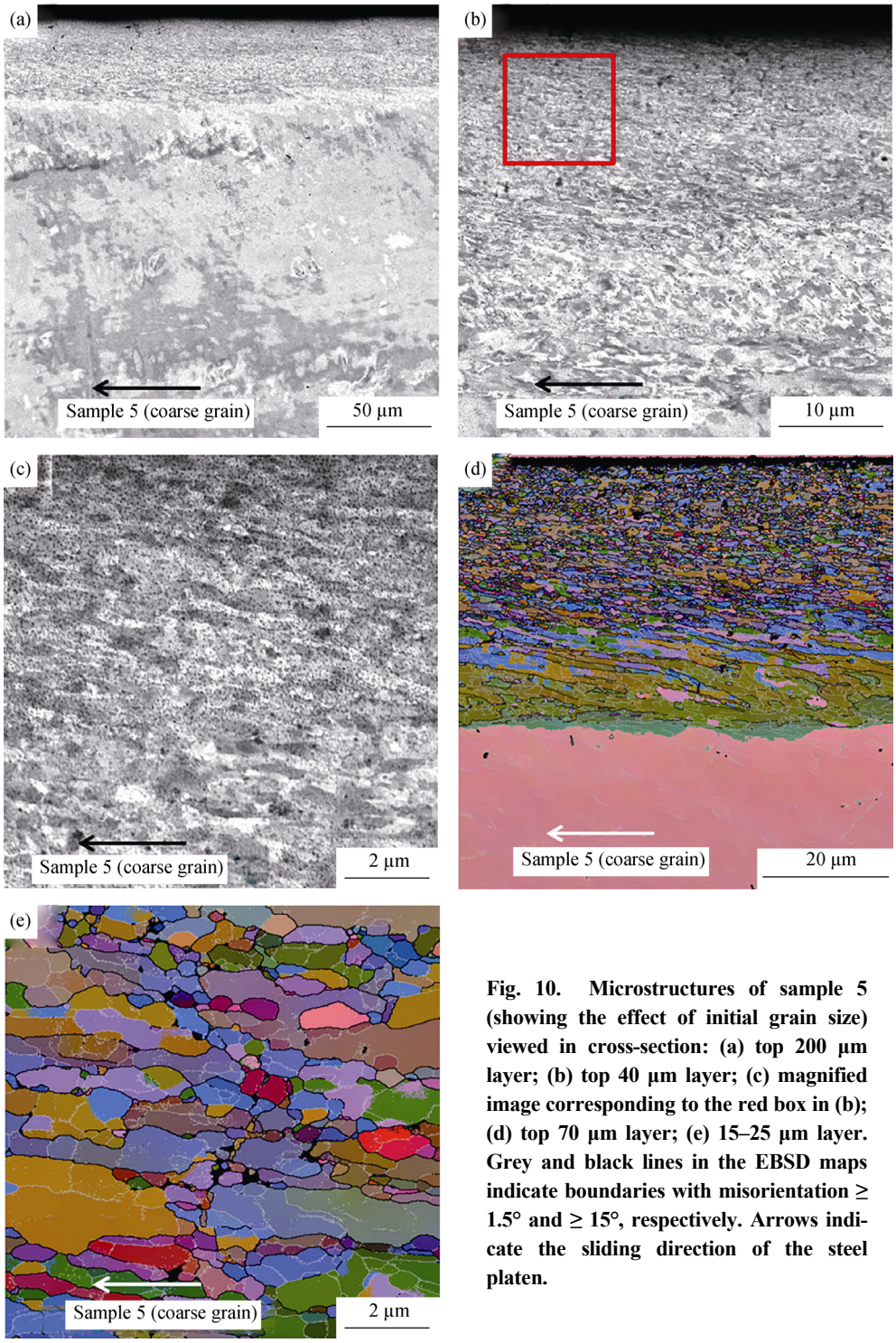

Fig. 10. Microstructures of sample 5 (showing the effect of initial grain size) viewed in cross-section: (a) top 200 μm layer; (b) top 40 μm layer; (c) magnified image corresponding to the red box in (b); (d) top 70 μm layer; (e) 15–25 μm layer. Grey and black lines in the EBSD maps indicate boundaries with misorientation ≥ 1.5° and ≥ 15°, respectively. Arrows indicate the sliding direction of the steel platen.

observed, where the grains are only weakly deformed. All these observations indicate that the transition from the fine-grain microstructure to undeformed material is much sharper than that in samples with conventional grain sizes.

3.4.2. Spacing and hardness

Fig. 11 compares the spacing of high-angle boundaries at 20 μm depth and the hardness at a certain depth between sample 5 and sample R. As immediately evident in the figure, the spacing between high-angle boundaries at 20 μm depth in sample 5 is larger than that in sample R (Fig. 11(a)), which is consistent with the microstructures shown in Figs. 10(e) and 3(e). The hardness values at depths of 40 μm and 20 μm and at the friction surface in sample 5 are, however, all slightly larger than those in sample R (Fig. 11(b)).

To explore this apparent discrepancy, we analyzed the microstructures at 20 μm depth in sample R and sample 5 in greater detail. Fig. 12 shows EBSD boundary maps (plotting all misorientations ≥ 1.5°) of the same areas in Figs. 3(e) and 10(e). As shown in Fig. 12, most of the fine grains in sample R are very clean (i.e., they do not contain interior boundaries or boundary segments, indicated in the maps as short lines or black points, respectively). However, many of the fine grains in sample 5 show evidence of interior misorientations, and regions with a large number of small-angle misorientations exist. The fractions of high-angle boundaries in sample R and sample 5 for these maps are 61% and 44%, respectively. Therefore, the microstructure at 20 μm depth in sample 5 appears to be in a less dynamically recovered state compared to that in sample R; it also appears to contain more low-angle dislocation boundaries that will also contribute to the strength. As a consequence, sample 5 is expected to exhibit a slightly greater hardness.

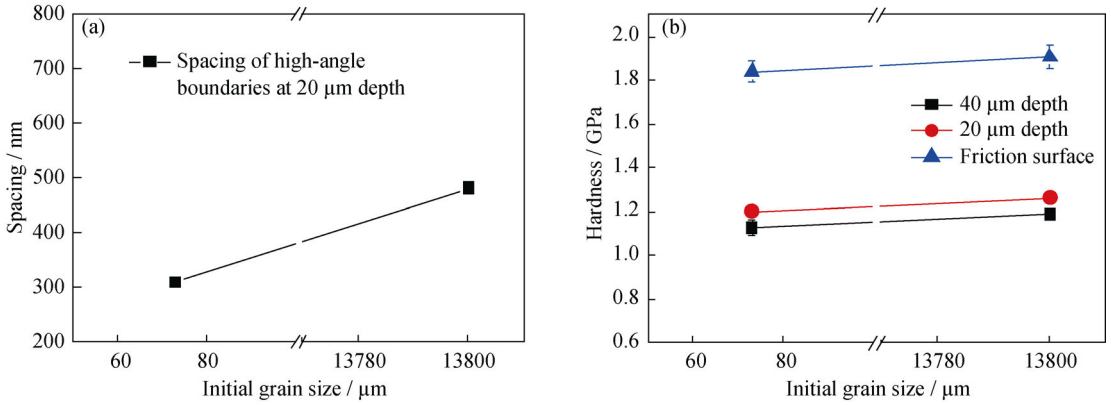

Fig. 11. Effect of initial grain size: (a) spacing of high-angle boundaries at 20 μm depth; (b) hardness at a fixed depth for samples with different initial grain sizes.

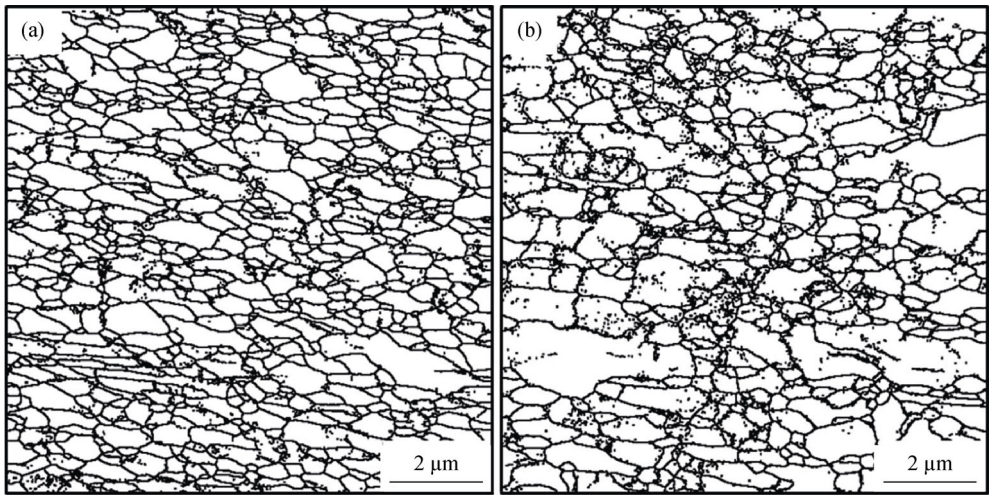

Fig. 12. Fine step-size EBSD boundary misorientation maps of areas shown in Figs. 3(e) (a) and 10(e) (b) showing boundary misorientation ≥ 1.5°.

The effect of the initial grain size on the grain refinement in a multi-impact process has been investigated [25]. The results of this previous study demonstrate that a larger initial grain size will result in more heterogeneous deformation compared to a smaller initial grain size. Therefore, for the large grain size case, the plastic deformation is more concentrated at the top surface layer, which directly interacts with the steel platen. Severe grain refinement only occurs in this thin top surface layer. As a result, the maximum depths at which the fine grains and regular lamellae are observed are all smaller and the transition from a fine-grain microstructure to undeformed material is sharper compared to the transition in the sample with a smaller initial grain size.

3.5. Microstructural control during PFSD

A key reason why surface severe plastic deformation (SPD) methods have attracted extensive scientific interest is that they enable mechanical properties to be enhanced

through optimization of the microstructure in the near-surface layer of processed samples, and especially at the top surface. PFSD is a novel surface SPD technique that can apply large shear deformation with high efficiency (i.e., with a short processing time) to a treated surface and therefore may be of interest for a wide range of engineering materials. Control of the microstructure generated by PFSD is therefore very important, both for improving (and ideally optimizing) material properties and for extending the range of potential engineering applications.

In the present study, the effects of normal stress, surface roughness, and initial grain size on the microstructure in Cu after PFSD processing were investigated. By changing these parameters, we obtained different microstructures in the surface layer after PFSD processing. An increase in the thickness of the overall deformed layer, as well as in the depth of the microstructure characterized by fine grains, can be achieved using a larger normal stress. In addition, the generation of nanoscale lamella microstructure in the very top layer can be promoted by decreasing the Cu sample surface roughness or by using a larger normal stress. Furthermore, a sharper transition from the fine-grained layer to undeformed material can be promoted by increasing the initial grain size of the sample, resulting in a structure in which the top surface layer with a certain thickness is severely refined while the microstructure beneath this layer is only moderately affected compared to the pre-PFSD condition.

4. Summary and conclusions

The effects of normal stress, surface roughness, and initial grain size on the microstructure in Cu after PFSD processing were examined. The major conclusions are summarized as follows:

(1) An increase in the amount of severe plastic deformation introduced by PFSD can be achieved by applying a larger normal stress. This is reflected in three aspects: (a) a thicker layer of fine grains is obtained, and shearing occurs to greater depths; (b) above a threshold value of the applied normal stress, a nanoscale lamella microstructure is formed at the sample surface layer, and the thickness of this layer increases with increasing normal stress; and (c) the hardness at any depth is increased, although the main increase occurs at the top surface.

(2) A decrease in the steel platen surface roughness significantly retards the microstructural evolution because less plastic deformation is introduced, as indicated by both a large decrease in hardness and the absence of a fine-grained layer. In contrast, a decrease of the Cu sample surface roughness enhances the formation of a gradient nanostructure, as evident by the formation of a thicker nanoscale lamella layer and an increase of hardness.

(3) Application of PFSD processing to a Cu sample with a much larger initial grain size results in a structure with a similar fine-grained layer (in terms of high-angle boundary spacing) but with a much sharper transition from the fine-grain microstructure to undeformed material in deeper volumes.

Acknowledgements

The authors gratefully acknowledge the support from the Danish National Research Foundation (Grant No. DNRF86-5) and the National Natural Science Foundation of China (Grant Nos. 51261130091 and 51171085) to the Danish–Chinese Center for Nanometals.

References

[1] X.D. Zhang, N. Hansen, Y.K. Gao, and X.X. Huang, Hall-petch and dislocation strengthening in graded nanostructured steel, *Acta Mater*, 60(2012), No. 16, p. 5933.

[2] X.C. Liu, H.W. Zhang, and K. Lu, Strain-induced ultrahard and ultrastable nanolaminated structure in nickel, *Science*, 342(2013), No. 6156, p. 337.

[3] X.Y. Wang, X.F. Liu, W.J. Zou, and J.X. Xie, Copper foils with gradient structure in thickness direction and different roughnesses on two surfaces fabricated by double rolling, *Int. J. Miner. Metall. Mater.*, 20(2013), No. 12, p. 1170.

[4] C. Ye, A. Telang, A.S. Gill, S. Suslov, Y. Idell, K. Zweiacker, J.M.K. Wiezorek, Z. Zhou, D. Qian, S.R. Mannava, and V.K. Vasudevan, Gradient nanostructure and residual stresses induced by ultrasonic nano-crystal surface modification in 304 austenitic stainless steel for high strength and high ductility, *Mater. Sci. Eng. A*, 613(2014), p. 274.

[5] Y.S. Zhang, Z. Han, K. Wang, and K. Lu, Friction and wear behaviors of nanocrystalline surface layer of pure copper, *Wear*, 260(2006), No. 9-10, p. 942.

[6] B.N. Mordyuk, G.I. Prokopenko, M.A. Vasylyev, and M.O. Iefimov, Effect of structure evolution induced by ultrasonic peening on the corrosion behavior of aisi-321 stainless steel, *Mater. Sci. Eng. A*, 458(2007), No. 1-2, p. 253.

[7] J.C. Villegas, L.L. Shaw, K. Dai, W. Yuan, J. Tian, P.K. Liaw, and D.L. Klarstrom, Enhanced fatigue resistance of a nickel-based hastelloy induced by a surface nanocrystallization and hardening process, *Philos. Mag. Lett.*, 85(2005), No. 8, p. 427.

[8] T. Roland, D. Retraint, K. Lu, and J. Lu, Fatigue life improvement through surface nanostructuring of stainless steel by means of surface mechanical attrition treatment, *Scripta Mater.*, 54(2006), No. 11, p. 1949.

[9] X. Wang, D.D. Mao, X.C. Wei, and W.R. Wang, Cr atom

diffusion in tribolayer T10 steel induced by dry sliding against 20CrMnTi steel, *Appl. Surf. Sci.*, 270(2013), p. 145.

[10] H.W. Huang, Z.B. Wang, X.P. Yong, and K. Lu, Enhancing torsion fatigue behaviour of a martensitic stainless steel by generating gradient nanograined layer via surface mechanical grinding treatment, *Mater. Sci. Technol.*, 29(2013), No. 10, p. 1200.

[11] D.A. Hughes, D.B. Dawson, J.S. Korellis, and L.I. Weingarten, Near surface microstructures developing under large sliding loads, *J. Mater. Eng. Perform.*, 3(1994), No. 4, p. 459.

[12] D.A. Hughes, D.B. Dawson, J.S. Korellis, and L.I. Weingarten, A microstructurally based method for stress estimates, *Wear*, 181-183(1995), No. 2, p. 458.

[13] Y.S. Zhang, W.L. Li, G. Wang, L.C. Zhang, B. Yao, and Z. Han, Formation of thick nanocrystalline surface layer on copper during oscillating sliding, *Mater. Lett.*, 68(2012), p. 432.

[14] Y.S. Zhang, P.X. Zhang, H.Z. Niu, C. Chen, G. Wang, D.H. Xiao, X.H. Chen, Z.T. Yu, S.B. Yuan, and X.F. Bai, Surface nanocrystallization of Cu and Ta by sliding friction, *Mater. Sci. Eng. A*, 607(2014), p. 351.

[15] X. Wang, X.C. Wei, X.R. Yang, Z.B. Cheng, and W.R. Wang, Atomic diffusion of gradient ultrafine structured surface layer produced by T10 steel rubbing against 20CrMnTi steel, *Wear*, 304(2013), No. 1-2, p. 118.

[16] J.R. Jiang, F.H. Stott, and M.M. Stack, A mathematical model for sliding wear of metals at elevated temperatures, *Wear*, 181-183(1995), No. 1, p. 20.

[17] B. Yao, Z. Han, and K. Lu, Correlation between wear resistance and subsurface recrystallization structure in copper, *Wear*, 294-295(2012), p. 438.

[18] S. Karthikeyan, H.J. Kim, and D.A. Rigney, Velocity and strain-rate profiles in materials subjected to unlubricated sliding, *Phys. Rev. Lett.*, 95(2005), No. 10, p. 10601.

[19] A. Emge, S. Karthikeyan, and D.A. Rigney, The effects of sliding velocity and sliding time on nanocrystalline tribolayer development and properties in copper, *Wear*, 267(2009), No. 1-4, p. 562.

[20] D.A. Hughes and N. Hansen, Exploring the limit of dislocation based plasticity in nanostructured metals, *Phys. Rev. Lett.*, 112(2014), No. 13, p. 135504.

[21] S.Q. Deng, A. Godfrey, W. Liu, and C.L. Zhang, Microstructural evolution of pure copper subjected to friction sliding deformation at room temperature, *Mater. Sci. Eng. A*, 639(2015), p. 448.

[22] A. Kumar, T. Staedler, and X. Jiang, Effect of normal load and roughness on the nanoscale friction coefficient in the elastic and plastic contact regime, *Beilstein. J. Nanotech.*, 4(2013), p. 66.

[23] K. Yamaguchi, C. Sasaki, R. Tsuboi, M. Atherton, T. Stolarski, and S. Sasaki, Effect of surface roughness on friction behaviour of steel under boundary lubrication, *Proc. Inst. Mech. Eng. Part J J. Eng. Tribol.*, 228(2014), No. 9, p. 1015.

[24] D.K. Leu, Modeling of surface roughness effect on dry contact friction in metal forming, *Int. J. Adv. Manuf. Technol.*, 57(2011), No. 5, p. 575.

[25] W. Chen, L. Xiao, Q.Y. Sun, and J. Sun, Effect of the initial grain size on grain refinement in Ti–2Al–2.5Zr alloy subjected to multi-impact process, *Mater. Sci. Eng. A.*, 554(2012), p. 86.